On Timing Reacquisition and Enhanced Primary Synchronization Signal (ePSS) Design for Energy Efficient 3GPP LTE MTC

Naveen Mysore Balasubramanya, Lutz Lampe, Gustav Vos and Steve Bennett

Abstract—Machine Type Communications (MTC) is one of the major drivers for the future growth of the Third Generation Partnership Project (3GPP) Long Term Evolution (LTE)/LTE-Advanced (LTE-A) standards. A primary challenge associated with MTC using LTE/LTE-A is to cater to varied requirements of the User Equipment (UE) like coverage enhancement, low complexity, low power consumption, etc. The current LTE/LTE-A standards incorporate the Discontinuous Reception (DRX) mechanism for reduced energy consumption where the UE wakes up periodically to check for a paging message from the base-station. On each wake-up occasion, the UE has to decode the paging information, which requires accurate timing resynchronization. In the case of the MTC UEs, especially when the devices are deployed in low coverage areas, the resynchronization consumes significant amount of time which increases the ON time of the UE leading to higher energy consumption. In this paper, we introduce the Enhanced Primary Synchronization Signal (ePSS) within the LTE/LTE-A standardization framework and propose a novel DRX mechanism which uses our ePSS for faster resynchronization and reduced energy consumption. We demonstrate that our mechanisms are more energy efficient than the legacy DRX mechanism for the MTC UEs with coverage enhancement.

Index Terms—Long Term Evolution (LTE), LTE-Advanced (LTE-A), Machine Type Communications (MTC), Machine-to-Machine (M2M), Internet of Things (IoT), Discontinuous Reception (DRX), Paging.

1 Introduction

The world is evolving towards an Internet of Things (IoT) where a large number of devices interact to realize different applications that constitute smart electricity grids, intelligent transportation systems, ubiquitous healthcare solutions, etc. Machine Type Communications (MTC) or Machine-to-Machine (M2M) communications provide the substrate for the connectivity and service mechanisms of these devices. Many services associated with the MTC applications such as smart metering, building security monitoring and reporting, location tracking, etc. require the cellular network as the backbone for communication. The 3rd Generation Partnership Project (3GPP) has recognized MTC as one of the principal components in driving the growth of cellular network and instituted the standardization of MTC from Release 11 of the Long Term Evolution (LTE) standard [1].

The challenges in MTC depend on the application for which the MTC device is being used. For example, the MTC devices used for smart metering require an efficient communication and service mechanism to operate in a low mobility, high delay tolerant, low data rate environment. These requirements are different from those of human-to-human (H2H) communications like video streaming on smartphones which require high data rate and low delay tolerance. The current LTE/LTE-A networks are designed for efficient H2H communications and the network architecture needs to be revamped to support MTC applications [2], [3], [4], [5], [6]. Also, the energy consumption of the MTC devices forms an integral part of the design of the MTC mechanisms [7].

Considering the application diversity and the variety of MTC network scenarios envisioned over the IoT platform, it would be difficult to have a single solution to answer the requirements of all the applications. Moreover, MTC devices can be placed in underground parking lots or basements of shopping malls where the network coverage is low. Therefore, the MTC mechanisms should be designed to work effectively for devices experiencing low coverage too. Small-cell based IoT solutions are prominent candidates in this regard, but they come at the expense of additional cost for network infrastructure/maintenance and backhaul provisioning and it is essential to have cost-effective solutions addressing the requirements of "hard to reach" devices in the network [8]. Although there is no consensus on the percentage of such devices in the network, forecasts indicate that they can be significant. For example, in [9], it is predicted that between 2015 and 2020, cellular M2M connections will grow from 310 million to 715 million and Low Power Wireless Access (LPWA) M2M connections will grow from 20 million to over 860 million. Moreover, smart meters are expected to be the largest LPWA application with a projected share of 45% of the total LPWA connections by 2020 [9]. Furthermore, low cost and extended coverage are the key features of LPWA technologies [8].

The 3GPP has classified such low-power, low-complexity MTC devices as Category-M (CAT-M) devices and has limited the maximum date rate supported by these devices to

Naveen Mysore Balasubramanya and Lutz Lampe are with the Department of Electrical and Computer Engineering, University of British Columbia, Vancouver, Canada. Gustav Vos and Steve Bennett are with Sierra Wireless Inc., Richmond, BC, Canada. *This work is supported MITACS, Canada and Natural Sciences and Engineering Research Council of Canada (NSERC).*

1Mbps [10], [11]. The design and development of MTC mechanisms for "hard to reach" devices has been recognized as a "work item" by the 3GPP under the label coverage enhancement (CE). The 3GPP has proposed to enable 15dB additional coverage in Release 13 of the LTE/LTE-Advanced (LTE-A) standards for MTC [10], [11].

1.1 Motivation

In a typical wireless communication system, it is important for the mobile device, or the so called user equipment (UE) to maintain accurate symbol timing synchronization with the base-station in order to decode the downlink data. The current Orthogonal Frequency Division Multiplexing (OFDM) based systems like LTE/LTE-A and Wireless local Area Network (WLAN) support power saving modes, where the UE is in sleep state when it is not transmitting or receiving data. It wakes up periodically to check whether it has a message (called the paging message) from the base-station. When the UE is in the sleep state, its clock drifts away from the nominal timing value. Therefore, every time the UE wakes up, it has to reacquire the symbol timing before checking for the paging message from the base-station.

The amount of clock drift depends on the quality of the oscillator used for the UE's clock. If the UE uses a high quality oscillator, the timing drift will be small. This means that the UE can sleep for a longer duration without losing the timing synchronization. Typically, mobile devices like smartphones using a high quality Voltage Controlled Temperature Compensated Crystal Oscillator (VCTCXO) have an accuracy of $\pm$1ppm [12]. But, the low-complexity MTC UEs cannot incorporate a high quality oscillator for its clock since it increases the cost of the device. Hence, most of them use a Voltage Controlled Crystal Oscillator (VCO) for their clock, which has an accuracy of $\pm$10ppm [13]. As an example, assuming that the symbol time is 72μs and the tolerable timing drift is 5%, i.e. 3.6μs, the MTC UE with a 10ppm accurate clock can sleep up to $\frac{3.6\mu s}{10.10^{-6}} = 0.36s= 360$ms, while the device with a 1ppm accurate clock can sleep up to $\frac{3.6\mu s}{1.10^{-6}} = 3.6$s. However, the sleep time supported by the network can be longer. For example, in LTE/LTE-A, the sleep time supported by the network has been recently extended to 2621.44s (43.69 minutes) [14]. Therefore, the assumption of perfect timing synchronization is not always true for both types of devices and timing reacquisition becomes important for successful communication between the UE and the base-station.

Conventionally, in OFDM based systems, the UEs reacquire the timing using cyclic prefix (CP) autocorrelation [15], [16] and/or by detecting the synchronization reference signals [17], [18], [19], [20] which are transmitted periodically by the base-station. The reacquisition time is inversely proportional to the Signal-to-Noise Ratio (SNR). In the case of the MTC UEs located in low coverage areas, the SNR at the UE receiver is as low as -14dB, thereby increasing the reacquisition time. Moreover, at such low SNRs, the time taken by the UE to decode the paging message is also significant, since the UE requires multiple repetitions of the paging message to decode it successfully. The increase in the reacquisition time and the paging message decode time lead to an increase in the ON time of the UE, thereby increasing the UE energy consumption.

Furthermore, the network has to accommodate for a large number of MTC devices in IoT scenarios. As a consequence, the base-station has to transmit the paging information to a large set of UEs and the probability that a UE is paged during each wake-up occasion decreases. However, the UE continues to check for paging information every time it wakes up, which consumes a substantial amount of energy. Therefore, it is vital to reduce the reacquisition time and the paging message processing time, especially when there is no page for the UE.

Our objective is to design mechanisms for faster timing reacquisition and simplified paging message processing mechanisms to reduce the energy consumption of the MTC UEs using LTE/LTE-A. In particular, we consider low-power, low-complexity MTC UEs requiring coverage enhancement, which are referred to as low coverage (LC) devices. Table 1 summarizes the LTE nomenclature and their usage throughout this paper.

1.2 Prior Work

The aspects of energy efficiency of the MTC UEs has been addressed in several works. In [21], [22], energy efficient mechanisms have been designed for the MTC UE operation in the uplink, but these solutions do not consider the CE mode of operation. The challenges associated with coverage enhancement in LTE/LTE-A uplink are discussed in [23], [24], [25] and novel UE transmission mechanisms are proposed to improve the decoding of UE data. The mechanisms to improve the coverage of the broadcast channel are described in [25] and a new design for the control channel for better performance in low coverage is proposed in [26]. However, these works do not examine the UE power consumption.

In order to reduce the power consumption of the UE, the Discontinuous Reception (DRX) mode of operation is adopted by the present LTE/LTE-A standards in the downlink. In this mode, the UE alternates through sleep and wake-up cycles and checks for the paging information from the base-station during its wake-up time [27], [28], [29], [30]. The power savings obtained from this procedure depend on the duration for which the UE is awake, i.e, the ON time of the UE, that in-turn depends on the procedure followed by the UE for decoding the paging information. The procedure for paging decode in LTE/LTE-A is computationally intensive, since the UE has to hypothesize over 44 blind decoding options to obtain the paging identifier on the control channel and then decode the data channel to get the paging data [29], [30], [31]. The 3GPP standardization committee is in the process of defining a new control channel (M-PDCCH) for LC devices so that the number of blind decodes required to detect the paging identifier on the control channel is reduced [14].

The analysis of power consumption for the UEs adopting the DRX mechanism has been studied earlier in [32], [33], [34], [35], [36], [37]. These works provide analytical models based on queuing theory and/or semi-Markov processes to illustrate the power consumption of the regular (non-CE) UEs in the DRX mode. In [38], the authors demonstrate

TABLE 1
LTE/LTE-A nomenclature and their usage in this paper

Acronym	Expansion	Usage
eNB	Evolved Node B	Base-station
PBCH	Physical Broadcast Channel	Broadcast channel
PDCCH	Physical Downlink Control Channel	Control channel
PDSCH	Physical Downlink Shared Channel	Data channel
CRS	Cell-Specific Reference Signal	Pilot signal
PSS SSS	Primary Synchronization Signal Secondary Synchronization Signal	Legacy synchronization signals
P-RNTI	Paging Radio Network Temporary Identifier	Paging identifier
CE MTC UE	Coverage Enhanced Machine Type Communication User Equipment	LC (low coverage) device

significant reduction in power consumption for the LC devices through a modified DRX mechanism where the device turns off its radio after transmission instead of checking for a page periodically. However, such a mechanism can be used only in the MTC applications that are transmit driven and cannot be used for the MTC UEs that require considerable downlink data from the base-station.

The performance of the control channel and the data channel has been analyzed in many prior works. For example, in [39], the control channel performance is analyzed for M2M traffic and the scenario of excess load on the control channel due to large number of MTC devices is discussed. In [40] and [41], the control channel Block Error Rate (BLER) performance is analyzed for various channel models and the data channel BLER performance is discussed in [42]. But these works assume perfect timing synchronization.

1.3 Contributions

In this paper, we examine the energy consumption of the MTC UEs in CE mode adopting the DRX mechanism supported by the current 3GPP LTE/LTE-A standards. The LC devices can spend a significant amount of energy to reacquire the timing owing to a very low operating SNR (around -14dB) and low quality VCOs used for their clocks. We explore the impact of timing reacquisition on the UE energy consumption and design a novel, fast resynchronization mechanism to improve the UE energy efficiency in the downlink.

Although the new control channel definition for LC devices can reduce computational complexity for decoding of the paging control information, the LC devices would still require multiple repetitions of the control information in order to successfully decode the paging identifier owing to the low operating SNR. Moreover, this decoding has to performed on each wake-up occasion of the DRX cycle, regardless of whether the device has a valid upcoming page or not, thereby increasing the energy consumption of the LC devices. To address this issue, we introduced the Quick Sleeping Indication (QSI) mechanism in our previous work [43], which suggests the UE to go back to "sleep" when it does not have an impending page. When such a QSI mechanism is adopted, the UE first decodes the QSI and only if the QSI indicates that there is an upcoming page, it will stay ON. Otherwise, it will go back to "sleep" immediately and save power. In this work, we propose a modified DRX mode of operation using the QSI in conjunction with our fast resynchronization mechanism for improved energy efficiency of the LC devices. The significant contributions of our work are as follows.

- We show that the legacy methods for resynchronization using CP autocorrelation and reference signal detection are not effective for the LC devices due to the increased ON time of the UE.
- We introduce our novel Enhanced Primary Synchronization Signal (ePSS) as the resynchronization signal for the LC devices and demonstrate the reduction in energy consumption when the ePSS is used for timing reacquisition during the DRX wake-up interval.
- We design and develop a new DRX mechanism where the ePSS can also be used as QSI that combines the advantages of the two schemes to provide faster timing reacquisition and quicker transition to sleep mode when there is no page begetting further improvement in the energy efficiency of the LC devices.
- We ensure that our solutions are designed such that the changes required to the current LTE/LTE-A standards are kept minimal and the resource allocation respects the procedure followed in the current standards.

The rest of the paper is outlined as follows. In Section 2, we briefly discuss the DRX and paging decode mechanism supported in the present 3GPP LTE/LTE-A standards. In Section 3, we demonstrate the importance of timing reacquisition for the MTC UE operation in CE mode and explore the conventional mechanisms for timing reacquisition. In Section 4, we describe the design and resource allocation aspects of our proposed ePSS mechanism and discuss how the ePSS can also be used as QSI to reduce the ON time of the MTC UE. In Section 5, we compare the detection performance of our ePSS signal and the legacy synchronization signal and illustrate the energy efficiency obtained when our ePSS is adopted by the LC devices in DRX. The conclusions are drawn in Section 6.

2 DRX MODES AND PAGING MECHANISM IN LTE/LTE-A

The 3GPP LTE/LTE-A standards adopt the DRX mechanism for reducing the power consumption of the UE. When a UE is in the DRX mode, it follows a periodic cycle called the DRX cycle involving sleep intervals and wake-up intervals. The current LTE/LTE-A standards support different DRX cycle lengths with a maximum length of 2.56s. Recently, extended DRX cycle lengths starting from 5.12s to a maximum of 2621.44s have been approved by the 3GPP [14]. In

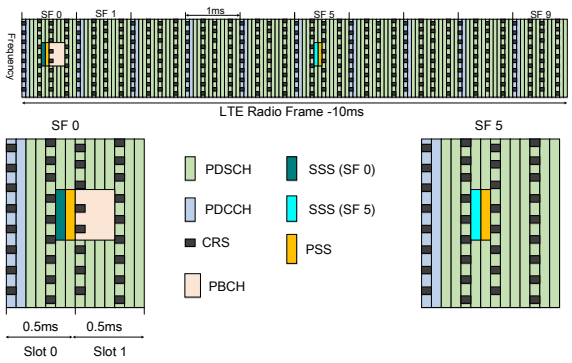

Fig. 1. LTE FDD radio frame structure showing the different LTE physical channels.

this section, we briefly review the DRX and paging decode mechanism in the current LTE/LTE-A standards.

Fig. 1 shows an LTE/LTE-A radio frame and the different physical channels supported by LTE/LTE-A. During each wake-up interval or the ON time, the UE looks for a page from the base-station [27], [28], [29]. The paging block in LTE/LTE-A consists of a paging identifier transmitted on the control channel and the paging data transmitted on the data channel [30], [44], [45]. The paging data indicates the list of UEs being paged using unique UE specific signatures [31]. A valid paging information is received by the UE if it is successful in decoding the paging identifier and the paging data block containing its unique signature[1]. The UE goes back to sleep if it does not get a valid page.

There are two modes of DRX operation supported in the present 3GPP LTE/LTE-A standards based on the Radio Resource Configuration (RRC) state - a) Connected Mode DRX and b) Idle Mode DRX [28], [29]. In the Connected Mode DRX, the UE traverses the DRX cycle by remaining connected at the RRC level, which is helpful to devices that access the network frequently such as smartphones. In this mode, the ON time of the UE is generally 100ms corresponding to 100 sub-frames in LTE/LTE-A. Since the control channel is transmitted on every sub-frame (see Fig. 1) and a control channel block with the paging identifier can be present on any of the 100 sub-frames, the UE may eventually process multiple control channel blocks before it receives a valid one.

In this work, we focus on the Idle Mode DRX [29] where the UE releases the RRC connection before going into sleep and reestablishes it on wake-up. This mode is applicable to low-power, low-complexity MTC devices that access the network intermittently. Here each UE is assigned one sub-frame per DRX cycle known as the Paging Occasion (PO). The UE checks for the control channel only on the PO sub-frame which is determined based on the UE Identifier (UEID) [27], [28], [29]. Hence, the ON time of the UE can be as small as 1ms in the ideal scenario where the UE timing is accurate and SNR is good. However, the MTC devices can be located in areas of bad network coverage, which results in low SNR at the UE receiver and requires more repetitions to decode the paging information. This increases the ON time of the UE, which results in increased energy consumption. Additionally, as discussed in Section 1, these low-complexity MTC UEs incorporate a low quality VCO for their clock in order to reduce the cost of the device, that causes a drift in the UE timing. This necessitates timing reacquisition that further increases the ON time and the energy consumption of the UE.

1. The paging identifier in LTE/LTE-A is called the Paging-Radio Network Temporary Identifier (P-RNTI) transmitted on the PDCCH and the unique UE specific signature corresponds to the System Architecture Evolution-Temporary Mobile Subscriber Identity (S-TMSI) or the International Mobile Equipment Identity (IMEI) data transmitted on the PDSCH.

TABLE 2
Simulation settings for Fig. 2.

Parameter	Setting
DL Bandwidth	1.4 MHz
Sampling Rate	1.92 MHz
Antenna Configuration	2×1
Channel Model	EPA
Max. Doppler Shift	1 Hz
MIMO Correlation	Low
PDCCH Settings	Type = Format 2 RNTI used = P-RNTI DCI Format = 1A
PDSCH Settings	MCS = 0 TBS = 16 bits Number of PRBs = 1

MCS: Modulation and Coding Scheme
TBS: Transport Block Size
PRB: Physical Resource Block

3 UE Timing Accuracy and Legacy Timing Acquisition Algorithms

In this section, we first demonstrate the sensitivity of the control channel/data channel paging decode operation to the UE timing offset. Then, we explore the timing estimation and synchronization algorithms used widely in OFDM based systems. We examine the performance of two algorithms - a) CP autocorrelation [15], [16] and b) Synchronization signal detection [17], [18], [19], [20] and determine their suitability for low-complexity MTC UEs in CE mode. The LTE toolbox in MATLAB was used for the simulations. The Extended Pedestrian A (EPA) 1Hz channel was chosen since it is the recommended channel model to study the performance of MTC in LTE/LTE-A [10], [46] because it models the low mobility multi-path scenario quite well. Especially for the MTC UEs in low coverage, the 3GPP envisions the scenario where a significant portion of these devices are located in basements of buildings or underground parking lots and are mostly stationary, which is well characterized by the EPA 1Hz channel model [10], [46]. The Carrier Frequency Offset (CFO) value for timing reacquisition was chosen to be 1kHz [10]. But for the control channel and the data channel decoding, the CFO was set to 100Hz, since the initial CFO will be estimated and compensated after timing reacquisition and one has to account only for the residual CFO [10]. The other important simulation parameters are summarized in Table 2.

3.1 Importance of UE timing accuracy

The first step of the paging decode process is to check for the paging identifier by decoding the control channel. If

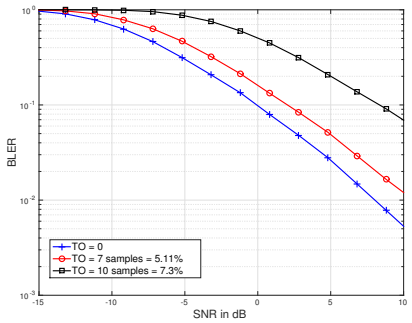

(a) Control channel BLER performance

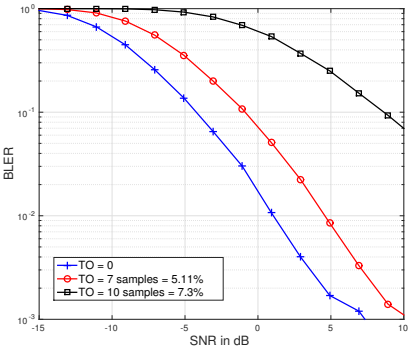

(b) Data channel BLER performance

Fig. 2. Illustration of the sensitivity of the control channel and the data channel decoding to timing offset (TO).

the paging identifier is found, the UE decodes the data channel to check for the paging data. Otherwise, it goes back to sleep. It is important to analyze the sensitivity of the control channel and the data channel performance with respect to UE timing accuracy. Similar to the previous works in [41], [42], we use the BLER as the metric for analyzing the performance the control channel containing the paging identifier and a data channel block containing paging data.

Fig. 2a and Fig. 2b demonstrate the BLER performance of the control channel and the data channel respectively. It is evident that both the control channel and the data channel are highly sensitive to timing offset. We consider the 10% BLER point to analyze the performance as suggested in [10] for LTE/LTE-A MTC. At 10% BLER, the control channel performance is degraded by about 8dB for as little as 7.5% error in timing estimation and the corresponding degradation in the data channel performance is 12dB. However, when the timing estimate is within 5% of the actual value, the degradation is less than 3dB in both the cases. Therefore, the accuracy of UE timing plays a vital role in the success of the paging decode mechanism in LTE/LTE-A. Additionally, for the LC devices, the timing reacquisition algorithms would be required to provide accurate results at very low SNR. Next, we discuss the performance of legacy timing estimation algorithms for the LC devices operating at low SNRs.

3.2 Timing reacquisition using CP autocorrelation

In this method, the symbol start position is obtained by finding the location of the peak of the CP autocorrelation [15], [16], [31]. For the illustration of the performance of CP autocorrelation, we accumulate the correlation results only

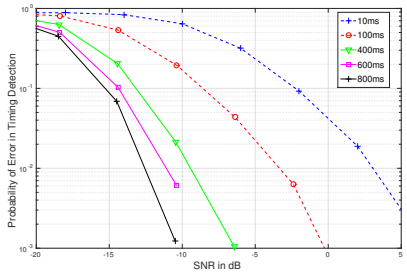

Fig. 3. CP autocorrelation performance.

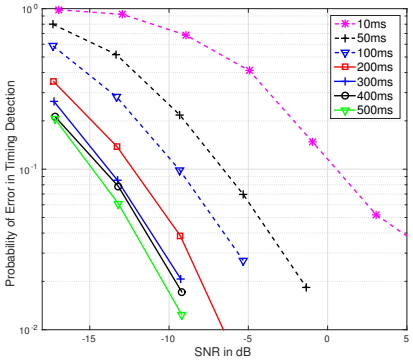

Fig. 4. Synchronization signal detection performance.

on the symbols that are used to transmit the pilot signal. This is because the pilot signal is always transmitted on specific symbols regardless of whether the base-station has data or control information to send. However, on the other symbols, the sub-carriers contain a valid signal only when they are used for control or data allocation. The pilot signal is transmitted on the first and fifth symbol of each slot (see Fig. 1) [31], [44].

Fig. 3 depicts the performance of CP autocorrelation for different accumulation times. For the LC devices, the operating SNR for the synchronization channel at 10% BLER is -14.2dB [10] and the error tolerance level of the estimated timing offset is set to $\pm 5\%$ based on the results obtained in Section 3.1. From Fig. 3, we observe that about 600 sub-frames (corresponding to 600ms) of accumulation time is required for 10% BLER at -14.2dB which is large. This is because there are only 9 CP samples available for correlation at a sampling rate of 1.92MHz (the sampling rate supported by the low-complexity MTC UEs [10]). This means that the MTC UE has to be on for 600ms (as discussed in Section 2) which will lead to increased energy consumption. Therefore, we conclude that the classical method of CP autocorrelation is not an efficient mechanism for timing reacquisition for low-complexity MTC UEs in CE mode.

3.3 Timing reacquisition using synchronization signal detection

The sub-frame synchronization in LTE/LTE-A standards is achieved by detecting the synchronization reference signals - the Primary Synchronization Signal (PSS) and the Secondary Synchronization Signal (SSS) [17], [31]. The PSS and the SSS occupy a bandwidth of 1.4MHz in the centre of the spectral band (see Fig. 1). The PSS is a Zadoff-Chu (ZC) sequence transmitted with a periodicity of 5ms. The PSS is transmitted on the last symbol of the first slot in sub-frame 0 and sub-frame 5 [30], [44], [45]. The UE can obtain

the 5ms sub-frame timing by detecting the PSS, but it will not know whether it is in the first half of the radio frame (corresponding to the detection of the PSS at sub-frame 0) or the second half (corresponding to the detection of the PSS at sub-frame 5). This ambiguity can be resolved by detecting the SSS which is transmitted one symbol before the PSS [30], [44], [45]. The SSS on sub-frame 0 is different from the one on sub-frame 5, and the UE can exactly determine the sub-frame number depending on the SSS pattern it detects [31].

For the synchronization signal detection, we consider the PSS and the SSS as one long sequence, since they are on consecutive symbols. For successful timing acquisition, we have to find the position of this sequence in a 10ms radio frame within a tolerance level (set to $\pm$5% in our implementation similar to Section 3.2). We use differential autocorrelation in frequency domain to detect the synchronization signal [17], [18].

Fig. 4 gives the performance results for timing reacquisition using the legacy synchronization signal detection. Considering 10% BLER at the coverage enhancement SNR of -14.2dB [10], we require around 400ms, i.e., 80 repetitions of the legacy synchronization signal to detect the correct timing offset. This is again significant, resulting in increased energy consumption of the UE. Therefore, we require a faster resynchronization mechanism to improve the energy efficiency of the LC devices.

4 Enhanced Primary Synchronization Signal

In this section, we introduce our new, simple resynchronization signal specially catering the needs of the LC devices. Since this signal is designed similar to the PSS, it would be apt to call it the enhanced PSS (ePSS). We discuss the design and resource allocation aspects of our ePSS mechanism.

4.1 ePSS Design

The ePSS signal should be designed such that the MTC UE can detect it with considerable accuracy at very low SNRs (around -14dB). Since the ePSS is used by LC devices, which have limited processing capabilities, it should be designed to provide robust detection with minimal complexity. This requires the ePSS signal to possess good autocorrelation and crosscorrelation properties. Such properties are demonstrated by the ZC sequences that are extensively used in the LTE/LTE-A standards, for example, in the case of the PSS in the downlink and the Physical Random Access Channel (PRACH) in the uplink. The ZC sequences are such that their cyclically shifted versions are orthogonal to each other and the crosscorrelation of two N length ZC sequences is limited by $\frac{1}{\sqrt{N}}$ [31]. These properties make them the perfect candidates for the ePSS signal design.

Also, the location of the ePSS in the LTE/LTE-A radio frame should be such that the UE can unambiguously determine the sub-frame number upon successful detection, which necessitates the ePSS to occupy exclusive and invariable resources in time and frequency. In order to obey the mandate of resource allocation dictated by the current LTE/LTE-A framework, such dedicated resources can be accommodated only in the data channel space. The number of symbols available for the data channel is decided by the base-station.

We use the data channel on sub-frames 1 and 2 for transmitting the ePSS, so that its location is fixed in time as shown in Fig. 5a. In LTE/LTE-A with normal CP, a sub-frame consists of 14 symbols. A Resource Element (RE) spans 1 sub-carrier $\times$ 1 symbol and a Physical Resource Block (PRB) consists of 12 REs $\times$ 7 symbols = 84 REs. The minimum unit of allocation spans 12 REs $\times$ 1 sub-frame, which corresponds to a pair of PRBs = 168 REs. A commonly used configuration for LTE/LTE-A MTC using normal CP is a sub-frame consisting of a 12 symbol data channel preceded by a 2 symbol control channel [10]. In this scenario, there are 168 - 2 $\times$ 12 = 144 REs per PRB pair available for the data channel. Also, some REs in the data channel are reserved for pilot signals, which is 12 REs per PRB pair in this case. This gives us 132 REs per PRB pair for the data channel.

In the extended CP case, a sub-frame consists of 12 symbols and the minimum unit of allocation spans 12 REs $\times$ 1 sub-frame = 12 $\times$ 12 = 144 REs. As in the case of normal CP, 12 REs per PRB pair are required for pilot signal transmission. Hence, the total number of REs available per PRB pair is 144-12 = 132 REs. Typically, one symbol is used for the control channel [10]. Therefore, we have 132 - 12 = 120 REs available for the data channel for the extended CP case.

In the following, we present two methods to design the ePSS - a) Using multiple PSS and b) Using new ZC sequences. The ePSS detection uses differential autocorrelation similar to the legacy synchronization signal detection mechanism discussed in Section 3.3.

4.1.1 ePSS construction using multiple PSS

In this method, the ePSS is formed by a burst of PSS copies occupying the REs in the data channel space. The advantage of re-using the existing PSS sequences is that they are readily available at the base-station and no additional processing/memory is required to generate/store a new sequence. An example for such an ePSS for normal CP is shown in Fig. 5b. An ePSS PRB consists of the concatenations of two PSS sequences of different roots. Unlike the regular PSS where the ZC sequence is spread across frequency, the PSS ZC sequence within our ePSS is spread across time (see Fig. 5b). This ensures that the legacy UEs do not falsely detect this signal as the PSS. The PSS signal is a 63-length ZC sequence [31] and two such sequences will occupy 126 REs. The unused REs are set to zero. The low-complexity MTC UEs can operate on a maximum DL bandwidth of 1.4MHz which corresponds to 6 PRBs. Therefore, we transmit 6 copies of the ePSS in a sub-frame which is equivalent to transmitting 12 PSS copies.

In the ePSS design, we cannot have the same signal on both sub-frame 1 and sub-frame 2, since the ePSS will be used for timing resynchronization. If these two sub-frames have the same signal, the UE would not be able to uniquely determine the sub-frame number. Therefore, we have to judiciously re-use the PSS sequences so that the two sub-frames are different, but can be detected together to uniquely determine the sub-frame number. The LTE/LTE-A standards use 3 roots for the PSS sequence - $r \in [r_0 = 25, r_1 = 29, r_2 = 34]$. Each ePSS sequence consists

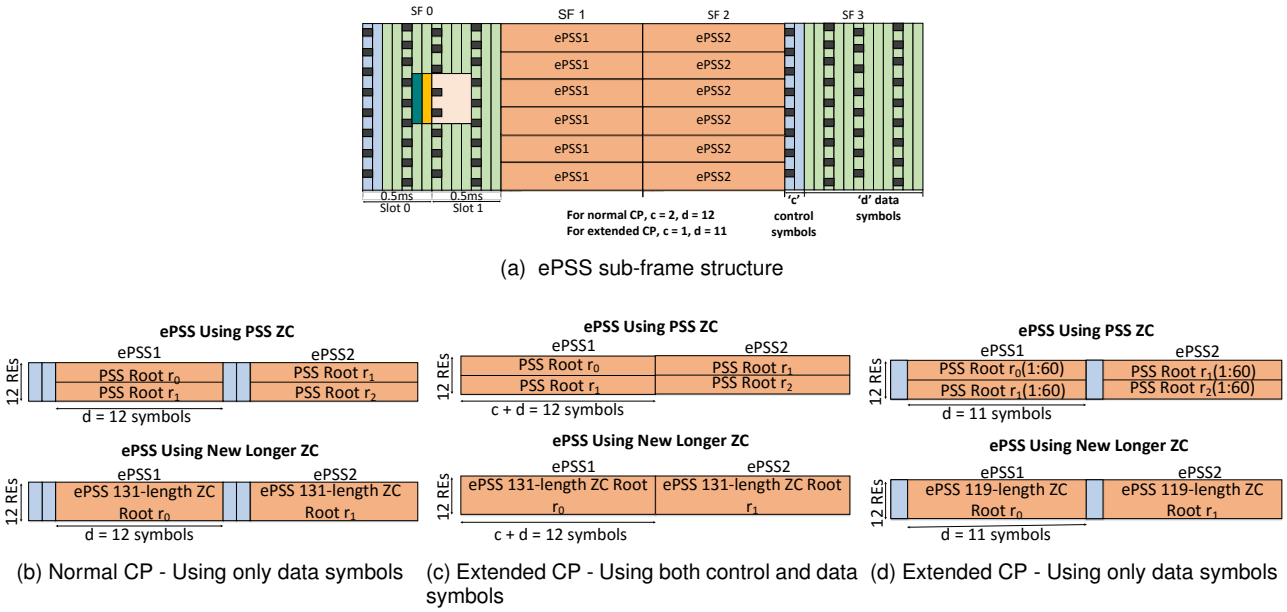

Fig. 5. Illustration of ePSS sub-frame structure for normal and extended CP

of 2 of the 3 possible PSS roots. This gives us 6 possible ways to choose the roots for sub-frame 1. They are (r_0, r_1), (r_0, r_2), (r_1, r_0), (r_1, r_2), (r_2, r_0) and (r_2, r_1).

Let us say that sub-frame 1 has the sequence (r_0, r_1) and call r_0 the top root and r_1 the bottom root. Since the ePSS is used for timing reacquisition, if both the sub-frames contain the same top and bottom roots, the UE using the ePSS to detect the timing will not know whether it detected the root on sub-frame 1 or on sub-frame 2. Therefore, we should have different sequences on sub-frame 1 and sub-frame 2. Hence, subfame 2 can only have (r_1, r_0), (r_1, r_2) or (r_2, r_0) as the sequence. Similarly, if we start with a different sequence for sub-frame 1, we have 3 possibilities for sub-frame 2. Thus, in total we have $6 \times 3 = 18$ sequences to construct the ePSS using this method.

Moreover, there are only 3 legacy PSS sequences and one sequence is used per sector. Therefore, the frequency reuse for the legacy scheme is 3, which may result in the detection of the neighbour PSS. However, for ePSS constructed using this method, we have 18 possible sequences (greater than 7). Therefore, the ePSS can be used with a frequency re-use factor of 7, which reduces the probability of the neighbour ePSS detection.

For the extended CP case, the ePSS transmission uses one of the following schemes - a) using both the control and data symbols (as shown in Fig. 5c) and b) using only the data symbols (as shown in Fig. 5d). In the first scheme, there are 132 REs available per PRB pair (since the control symbols are also used) and the ePSS sequences are the same as that for normal CP. However in the second scheme, there are 120 REs available per PRB pair and the ePSS sequences are slightly shortened so that they can be accommodated within the available space with negligible loss in performance.

4.1.2 ePSS construction using new ZC sequences

In this method, we use new ZC sequences for the ePSS instead of re-using the PSS ZC sequences. The ZC sequence is of the form $\mathrm{ZC}(r) = \mathrm{e}^{\left(\frac{-j\pi rn(n+1)}{N}\right)}$, where $n = 0, 1, \cdots N-1$, r is the root of the ZC sequence and N is the length. The root r and the length N are co-prime. As discussed earlier, for the PSS, $N = 63$ and $r \in [25, 29, 34]$. There are 33 more roots that are co-prime to 63 which can be used to construct new ZC sequences. The ePSS can be then constructed as described in Section 4.1.1. Our second solution for using new ZC sequences consists of using a longer length sequence for the ePSS. For example, in our scenario of using a data channel with 132 REs per PRB, we can use a ZC sequence of length 131 and set the single unused RE to zero. Also, using a longer length sequence provides a larger set of sequences since the number of roots co-prime with the length increases. Moreover, the cross-correlation between two ZC sequences is proportional to $\frac{1}{N}$ and a longer length sequence should improve the performance. Fig. 5b also depicts the construction of the ePSS using longer length ZC sequences for the normal CP case. Fig. 5c and Fig. 5d demonstrate the two ePSS transmission schemes for the extended CP case, where the former scheme uses the same 131-length ZC sequences as that of the normal CP and the latter uses a 119-length shortened ZC sequences.

Similar to Section 4.1.1, the signals on sub-frame 1 and sub-frame 2 should be different so that the MTC UE can clearly identify the sub-frame number on resynchronization. With a 131 length sequence, we have 130 possible roots and $130 \times 129 = 16{,}770$ sequences. This gives us a large set of sequences to choose for the ePSS signal design. Again, such an ePSS can also be used with a frequency re-use factor of 7 due to the availability of multiple sequences, which reduces the probability of detecting a neighbour ePSS.

4.2 ePSS Allocation

The ePSS will be used for resynchronization of the MTC UE with the same cell. Hence, the location(s) of the ePSS in the LTE frame structure should be known by the UE beforehand. Therefore, the ePSS cannot be scheduled using the control channel or the enhanced control channel (ePDCCH) [47]. We propose the following allocation schemes.

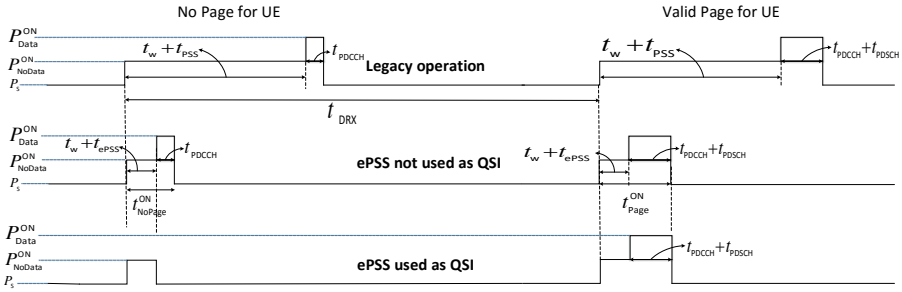

Fig. 6. Illustration of ON time and sleep time for UEs using the legacy and the ePSS based resynchronization mechanisms.

- **ePSS on centre band**: This is a fixed allocation scheme where the REs used for the ePSS always correspond to the centre band occupying 1.4MHz. The location of the ePSS in time is already fixed, i.e., on sub-frames 1 and 2 and it is transmitted every t_{p} seconds. This method is advantageous for the UE, because there is no additional signaling to indicate the location of the ePSS. The disadvantage is that it limits the flexibility of resource allocation optimization at the base-station, because it cannot use the ePSS REs for other data allocation at any scheduling interval.
- **ePSS on any contiguous band spanning 1.4MHz**: In this variant of ePSS allocation, we use any contiguous band spanning 1.4MHz within the available bandwidth at the base-station for the ePSS. The location of the ePSS can be broadcast within a System Information Block (SIB), which will be decoded by the UE when it connects to the cell initially and is updated every 3 hours [31]. This is feasible because the ePSS is only used for resynchronization, i.e., whenever the device wakes up from DRX and reacquires the timing. The initial synchronization is still done using the legacy synchronization signals. After initial synchronization, the device can decode the SIB, which will convey the ePSS location. Another way of conveying the location of the ePSS would be through higher layer signaling. Here, the initial location of the ePSS is obtained from SIB, but the subsequent location is indicated to the UE via higher layer signaling. This gives more flexibility for the base-station to optimize the resource allocation process.

4.3 ePSS as Quick Sleeping Indication (QSI)

Besides the time consumed by the MTC UE for resynchronization, it is highly possible that the UE can spend a significant amount of time and power trying to decode the paging control information on the control channel. This is because the LC devices require multiple repetitions to successfully decode the paging control information due to very low operating SNR.

The DRX procedure necessitates the UE to wake-up and look for paging during each PO. However, the probability that a UE is paged on every PO instance is very low since the network consists of a large number of UEs. Therefore, we introduced the Quick Sleeping Indication (QSI) mechanism for energy efficient DRX operation in our previous work [43]. The QSI mechanism assumes that the UEs are categorized into multiple groups. The QSI signal will indicate "sleep" if there is no impending page for the UE group, otherwise it will indicate "stay-awake". The UE decodes the QSI and attempts to decode the paging information only if the QSI indicates "stay-awake". Otherwise, it goes back to sleep immediately and saves power.

The earliest phase to indicate the presence or absence of a page is when it is resynchronizing with the base-station. Therefore, it would be beneficial if the resynchronization signal can also serve as the QSI signal. The ePSS signal presented in the previous section can fulfill this role as follows.

- The LC devices are divided into N_{grp} groups and assigned a pair of ePSS patterns denoted by $(ePSS_0, ePSS_1)$.
- The base-station schedules the POs one group at a time. It transmits $ePSS_0$ if the UE group is not paged in the subsequent PO. Otherwise, it transmits $ePSS_1$.
- When the UE attempts to resynchronize with the base-station, it hypothesizes over the two assigned patterns and detects one of them. If it detects $ePSS_0$, the UE interprets that there is no upcoming page in the PO and goes back to sleep immediately. If it detects $ePSS_1$, then it remains awake to decode the paging message.

Hence, the ePSS pattern can also serve as the QSI enabling the UE to resynchronize and go back to sleep quickly when there is no valid page.

Fig. 6 depicts the UE sleep and wake-up durations for the legacy mode of operation, when it uses the ePSS only for resynchronization (not as QSI) and when it uses the ePSS also as the QSI. The notations t_{DRX}, t_{PDCCH} and $t^{\mathrm{ON}}_{\mathrm{NoPage}}$ denote the length of UE DRX cycle, the ON time of the UE to decode the control channel and the total ON time of the UE when there is no page respectively. Since our ePSS mechanism is designed to provide faster timing reacquisition, the ON time of the UE decreases when it uses the ePSS for resynchronization instead of the legacy synchronization signal. Also, the UE ON time further reduces by a factor of $\frac{t_{\mathrm{PDCCH}}}{t^{\mathrm{ON}}_{\mathrm{NoPage}}}$ when the ePSS is also used as the QSI. A detailed discussion on the performance analysis of the ePSS is presented in the next section.

5 Performance Analysis

In this section, we analyze the detection performance of our ePSS mechanism and demonstrate that it is better than the legacy synchronization signal detection mechanism. We also provide a simple model based on the ON time to compute the energy consumption of the UE and show that the UEs adopting the DRX mechanism along with our ePSS for timing resynchronization consume much lesser energy than the UEs using the current DRX mechanism with legacy synchronization signal detection for resynchronization.

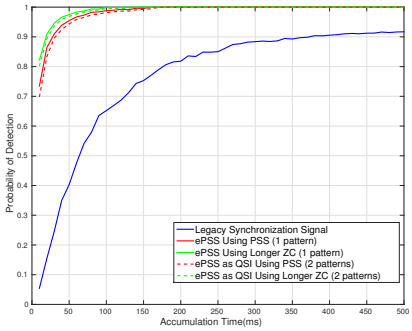

Fig. 7. Performance of legacy synchronization signal detection and ePSS detection.

TABLE 3
Rx energy efficiency gain for LC devices in DRX mode using ePSS.

DRX Length t_{DRX}	ePSS using multiple PSS		ePSS using new longer ZC	
	Not as QSI	As QSI	Not as QSI	As QSI
2.56s	3.9 - 7.6	9.9 - 11.5	4.3 - 9.3	12.6 - 16.0
5.12s	3.9 - 7.6	9.9 - 11.4	4.3 - 9.3	12.6 - 15.9
10.24s	3.9 - 7.5	9.8 - 11.3	4.3 - 9.2	12.4 - 15.7
327.68s	3.4 - 5.5	6.9 - 7.2	3.7 - 6.4	8.1 - 8.7
2621.44s	2.1 - 2.4	2.6 - 2.8	2.2 - 2.5	2.7 - 2.9

5.1 Reacquisition performance analysis

The ePSS solutions discussed in Section 4 were simulated with the settings listed in Table 2 and a CFO of 1kHz. The SNR considered for this simulation is -14.2dB, which corresponds to the operating SNR for the MTC UEs that require 15dB coverage enhancement [10]. The detection threshold is set such that the false alarm rate is limited to 1%. Fig. 7 shows the performance of the legacy synchronization signal detection scheme and our two ePSS design schemes (refer to Sections 4.1.1 and 4.1.2) along with the case where the ePSS is also used as the QSI (refer to Section 4.3). It is observed that the ePSS designed using longer length ZC sequences performs slightly better than the ePSS designed by re-using the PSS ZC sequences. As discussed in Section 4.1.2, the longer length ZC sequence has better cross-correlation properties that results in better performance.

In order to analyze the performance, we consider the accumulation time required for 90% detection denoted by t_{acc}. We note that the legacy synchronization signal detection requires $t_{\mathrm{acc}} = 380$ms that corresponds to 76 legacy synchronization signal repetitions, since it is transmitted every 5ms. In this simulation, the ePSS is transmitted on sub-frame 1 and sub-frame 2 of the radio frame. This set of two sub-frames is denoted as "ePSS Block". For the ePSS constructed using multiple PSS (refer to Section 4.1.1), $t_{\mathrm{acc}} = 30$ms that corresponds to 3 ePSS Blocks and for the ePSS constructed using longer length ZC sequences (refer to Section 4.1.2), $t_{\mathrm{acc}} = 20$ms corresponding to 2 ePSS blocks. Also, it is evident that there is negligible degradation in performance when the ePSS is also used as the QSI for both the mechanisms. The ePSS detection consumes less than 10% of the time taken by legacy synchronization signal detection for the LC devices, which decreases the ON time of the UE significantly and reduces the energy consumption.

5.2 Energy efficiency analysis

Now we analyze the energy consumption of the UE following the DRX mechanism when it uses the legacy synchronization signal detection for resynchronization and compare it to the energy consumption of the UE when it uses our ePSS solutions. In this work, we look at energy consumption from the physical layer perspective and consider a simple model for our energy consumption calculation based on two quantities - a) ON time of the UE and b) sleep time of the UE similar to [32].

Let t_{w} and t_{r} denote the time taken for the UE RF warm-up and the time taken for the UE resynchronization respectively. The UE ON time for the control channel decode and the ON time of the data channel decode are denoted by t_{PDCCH} and t_{PDSCH} respectively. P_{ON} and P_{S} represent the power consumed by the UE during the ON time and the sleep time respectively. In order to decode a page, the UE warms up, resynchronizes with base-station and decodes the control channel to check for a page. If the control channel contains paging identifier, the UE attempts to decode the paging data on the data channel. Otherwise, it goes back to sleep. Hence, the total ON time of the UE depends on whether it received a page or not. When the UE has a valid page, the ON time (see Fig. 6) is given by $t^{\mathrm{ON}}_{\mathrm{Page}} = t_{\mathrm{w}} + t_{\mathrm{r}} + t_{\mathrm{PDCCH}} + t_{\mathrm{PDSCH}}$ and the corresponding energy consumed is given by

$$E^{\mathrm{ON}}_{\mathrm{Page}} = (t_{\mathrm{w}} + t_{\mathrm{r}})P^{\mathrm{ON}}_{\mathrm{NoData}} + (t_{\mathrm{PDCCH}} + t_{\mathrm{PDSCH}})P^{\mathrm{ON}}_{\mathrm{Data}} \,. \quad (1)$$

where $P^{\mathrm{ON}}_{\mathrm{NoData}}$ and $P^{\mathrm{ON}}_{\mathrm{Data}}$ denote the ON time power consumption of the UE without active data and with active data respectively. The warm-up and resynchronization phases are considered to be non-active data phases since the UE is not running intricate control/data decoding processes like layer demapping, de-precoding. Viterbi/turbo decoding, etc. Therefore, the power consumption in these phases is $P^{\mathrm{ON}}_{\mathrm{NoData}}$.

When there is no page for the UE, the ON time (see Fig. 6) is determined by $t^{\mathrm{ON}}_{\mathrm{NoPage}} = t_{\mathrm{w}} + t_{\mathrm{r}} + t_{\mathrm{PDCCH}}$ and the corresponding energy consumed is given by

$$E^{\mathrm{ON}}_{\mathrm{NoPage}} = (t_{\mathrm{w}} + t_{\mathrm{r}})P^{\mathrm{ON}}_{\mathrm{NoData}} + t_{\mathrm{PDCCH}}P^{\mathrm{ON}}_{\mathrm{Data}} \,. \quad (2)$$

The sleep time can be obtained by subtracting the ON time from the total length of the UE DRX cycle (denoted by t_{DRX}). For the UE using the legacy synchronization signal detection, $t_{\mathrm{r}} = t_{\mathrm{PSS}}$, which is the time consumed for the legacy synchronization signal detection. For the UE using our ePSS for resynchronization, $t_{\mathrm{r}} = t_{\mathrm{ePSS}}$, which corresponds to the ePSS detection time. Also, when the ePSS is used as the QSI and when there is no page for the UE, the decoded ePSS pattern itself suggests that there is no valid page and the UE does not decode the control channel. In this case, the ON time will be $t^{\mathrm{ON}}_{\mathrm{NoPage}} = t_{\mathrm{w}} + t_{\mathrm{ePSS}}$. Using p to denote the probability that the UE is paged, the total energy consumed by the UE can be calculated as

$$\begin{aligned} E_{\mathrm{tot}} = {} & p \cdot (E^{\mathrm{ON}}_{\mathrm{Page}} + (t_{\mathrm{DRX}} - t^{\mathrm{ON}}_{\mathrm{Page}})P_{\mathrm{S}}) \\ & + (1-p) \cdot (E^{\mathrm{ON}}_{\mathrm{NoPage}} + (t_{\mathrm{DRX}} - t^{\mathrm{ON}}_{\mathrm{NoPage}})P_{\mathrm{S}}) \,. \end{aligned} \quad (3)$$

where P_{S} denotes the power consumed by the UE in deep sleep state.

For the Rx power consumption, we used $P_{\text{Data}}^{\text{ON}} = 500$mW, $P_{\text{NoData}}^{\text{ON}} = 250$mW and $P_{\text{S}} = 0.0185$mW [48], [49]. The UE warm-up time t_{w} was assumed to be 1ms and the paging rate $p = 0.1$. We used $t_{\text{PSS}} = 380$ms for the legacy synchronization signal detection, $t_{\text{ePSS}} = 30$ms for the ePSS using multiple PSS and $t_{\text{ePSS}} = 20$ms for the ePSS using longer ZC sequences corresponding to the accumulation time required for 90% detection (see Fig. 7). The energy efficiency gain indicates the ratio of the energy consumed by the UE receiver using the legacy synchronization signal detection for resynchronization to the energy consumed by the UE receiver using our ePSS for resynchronization. Table 3 summarizes the energy efficiency gain of the UE using our ePSS solutions for different values of the DRX cycle length t_{DRX}. We examined two scenarios - a) Short paging decode time assuming $t_{\text{PDCCH}} = t_{\text{PDSCH}} = 10$ms corresponding to the upper bound of the energy efficiency gains in Table 3 and b) Long paging decode time using $t_{\text{PDCCH}} = t_{\text{PDSCH}} = 40$ms corresponding to the lower bound of the energy efficiency gains in Table 3. The cases we examined include the maximum length of the DRX cycle supported in the current LTE/LTE-A standards (2.56s) and the maximum extended DRX cycle length (2621.44s).

In the following, we choose the DRX cycle length of 10.24s to illustrate the interpretation of the energy efficiency gains in Table 3. In this case, the UE adopting DRX with our ePSS using multiple PSS mechanism for resynchronization is 3.9 times (denoted by 3.9x) more energy efficient than the UE using DRX with the legacy synchronization signal detection mechanism for resynchronization owing to faster timing reacquisition using the ePSS. Also, the gain obtained from the ePSS using longer ZC sequences is higher compared to the ePSS constructed using multiple PSS (4.3x as opposed to 3.9x), since the ePSS using longer ZC sequences requires a lesser time for reacquisition.

Moreover, the energy efficiency improves further when the ePSS is used as the QSI. For example, in the case of the 10.24s DRX cycle, using our ePSS as QSI mechanisms are 9.8x (for the ePSS using multiple PSS) and 12.4x (for the ePSS using longer ZC sequences) more energy efficient than the legacy mechanism respectively. This demonstrates a significant increase compared to the corresponding gains obtained when the ePSS is not used as the QSI (3.9x and 4.3x respectively). This is because the LC device does not decode the control channel when the ePSS pattern indicates that there is no page (which happens 90% of the time since $p = 0.1$) unlike the non-QSI cases where the UE has to decode the control channel regardless of whether it is paged or not, thereby simplifying the operation of checking for a page when our ePSS as QSI mechanism is used.

A common trend observed with the different ePSS solutions is that the energy efficiency gain decreases with the increase in length of the DRX cycle. This is because the reduction in energy consumption is directly proportional to the fraction of the time the UE is ON during the DRX cycle. Since the ON time of the UE depends on the SNR and not on t_{DRX}, this ratio decreases with increase in t_{DRX} for a fixed SNR. However, even for the maximum DRX cycle length of 2621.44s, the energy efficiency gain obtained is between 2.1x and 2.5x when ePSS is not used as QSI, which is considerable and improves further (between 2.6x and 2.9x) when ePSS is used as QSI. Also, for longer DRX cycle lengths, the legacy UE may have to reacquire the system frame number (SFN) before attempting to decode the paging control information (as discussed later in Section 5.5), while the UE using our ePSS solutions (as QSI) is informed about an upcoming page during the timing resynchronization phase itself and need not decode the SFN when there is no page. The energy efficiency gain computation does not account for the ON time of the UE for SFN decoding. Therefore, the energy efficiency gains obtained using our ePSS as QSI solutions (columns 2 and 4 of Table 3) for longer DRX cycles serve as a loose lower bound for the actual gains.

5.2.1 Energy consumption due to UE computation

In a typical Digital Signal Processor (DSP), one real addition takes one operation and one real multiplication also requires one operation. Each accumulation is a complex addition and one complex addition uses two real additions. At a sampling rate of 1.92MHz (please see Table 2), we have 19200 samples in 10ms and each accumulation takes $19200 \times 2 = 38400$ operations. The signal detection is done in frequency domain. Since each subframe (1ms) contains 14 symbols for the case with normal CP, the 10ms buffer consists of 140 symbols. Using 128-point FFT (the FFT size corresponding to 1.4MHz bandwidth) and noting that an N-point FFT takes $4N\log_2(N) - 6N + 8$ operations [50], the number of operations consumed by FFT is $140 \times (4 \times 128 \times \log_2(128) - 6 \times 128 + 8) = 395360$. Similarly, correlating a signal with a reference involves L complex multiplications, followed by $L-1$ complex additions, where L is the length of the signal. Each complex multiplication involves 4 real multiplications and 2 real additions = 6 operations. Therefore, a correlation uses $6L + (L-1)2 = 8L - 2$ operations. The UE should perform this correlation on each symbol and find the symbol number that gives the best correlation energy. Therefore, correlation takes $140(8L - 2)$ operations. The total number of operations is the sum of accumulation, FFT and correlation operations.

In the legacy case, the known signal consists of one set of PSS and SSS on subframe 0 and the second set on subframe 5, each of length 63. Therefore, $L = 63 \times 4 = 252$. Also, the accumulation time required to detect the legacy synchronization signals is 380ms = 38 accumulations (please refer Fig. 7). The total number of operations for legacy synchronization signal detection is $38400 \times 38 + 395360 + 140(252 \times 8 - 2) = 2136520$. In our proposed solution, the UE looks for the ePSS signal transmitted on subframes 1 and 2. For ePSS using PSS, $L = 63 \times 24 = 1512$ since we use 24 PSS sequences for constructing the ePSS and the accumulation time is 30ms (3 accumulations). The total number of operations to detect the ePSS is 2203720. When ePSS is used as QSI, the correlation has to be performed for 2 patterns (one pattern indicating "sleep" and one indicating "stay-awake"). The accumulation and FFT operations remain the same. Then, the total number of operations for detecting ePSS using PSS (as QSI) is $38400 \times 3 + 395360 + 2 \times 140(1512 \times 8 - 2) = 3896880$. Similarly, for ePSS using new longer ZC sequences, $L = 131 \times 12 = 1572$, since we use 12 ZC sequences of length 131 and the accumulation time is 20ms (2 accumulations). The total number of operations for

TABLE 4
Battery Lifetime gain for LC devices using ePSS with $t_{\mathrm{DRX}} = 10.24$s and $t_{\mathrm{DRX}} = 2621.44$s.

Tx:Rx energy consumption share	ePSS using multiple PSS		ePSS using new longer ZC		ePSS using multiple PSS		ePSS using new longer ZC	
	Not as QSI	As QSI	Not as QSI	As QSI	Not as QSI	As QSI	Not as QSI	As QSI
	$t_{\mathrm{DRX}} = 10.24$s				$t_{\mathrm{DRX}} = 2621.44$s			
70:30	1.29 - 1.35	1.37 - 1.38	1.30 - 1.36	1.38 - 1.39	1.19 - 1.21	1.23 - 1.24	1.20 - 1.22	1.23 - 1.24
50:50	1.59 - 1.76	1.81 - 1.84	1.62 -1.80	1.85 - 1.88	1.35 - 1.41	1.44 - 1.47	1.38 - 1.43	1.46 - 1.49
30:70	2.09 - 2.54	2.69 - 2.76	2.16 - 2.66	2.81 - 2.90	1.58 - 1.69	1.76 - 1.82	1.62 - 1.72	1.79 - 1.85

detecting ePSS using new longer ZC sequences is 2232520 and 3992880 without and with QSI, respectively.

The power consumption of a DSP used for wireless applications [51] is 100 million operations per second (MOPS) per mW. In other words, the energy consumption is 1mJ for 100 million operations. Therefore, the legacy synchronization signal detection consumes $\frac{2136520}{100\times10^6} = 0.02137$mJ. Our ePSS using PSS detection consumes 0.02204mJ (not as QSI) and 0.03897mJ (as QSI). Our ePSS using new longer ZC sequences detection consumes 0.02233mJ (not as QSI) and 0.03993mJ (as QSI). However, the ON time of the UE for legacy synchronization signal detection is 380ms and the power consumption due to the radio being ON is 250mW, which corresponds to an energy consumption of $250 \times 10^{-3} \times 380 \times 10^{-3} = 95$mJ. For ePSS using PSS, the ON time radio energy consumption is 7.5mJ (for 30ms ON time) and for ePSS using new longer ZC sequences, it is 5mJ (for 20ms ON time). It can be clearly seen that the energy consumption due to UE computation is much smaller than that of the ON time radio energy consumption. Therefore, the effect of UE computational energy on the energy efficiency would be negligible. Hence, the energy consumed by the UE computation block was not included in our calculations.

5.3 Battery Lifetime Improvement

Having established that the ePSS mechanisms result in higher energy efficiency, we now estimate the improvement in the battery lifetime of the device when our different ePSS solutions are used. The UE consumes its battery for both transmission and reception. The battery consumption share between UE's transmission and reception varies depending on the UE's application. For example, a device used for location tracking has to transmit the data more frequently than that used for smart meter data reporting. In both these applications require the device to periodically listen to the network to remain connected. The battery consumption share for transmission is higher for the UE used for location tracking, since it transmits data more frequently. However, for the UE used for smart meter data reporting, the battery consumption share is dominated by periodic reception. In the following, we analyze the improvement in battery life for three different scenarios based on ratio of the UE battery consumption for transmission to that of the reception - a) 70:30 (Tx $>$ Rx), b) 50:50 (Tx $=$ Rx) and c) 30:70 (Tx $<$ Rx).

Since our ePSS mechanisms are adopted by the UEs in the downlink, the energy efficiency gains obtained using our solutions is applicable to the UE reception. The battery lifetime gain is calculated as

$$\beta = \frac{1}{s_{\mathrm{Tx}} + \frac{s_{\mathrm{Rx}}}{\eta}} \tag{4}$$

where s_{Tx} and s_{Rx} indicate the UE battery consumption share for transmission and reception respectively, and η is the gain obtained by the use of our different ePSS solutions (given in Table 3). For example, in the first scenario $s_{\mathrm{Tx}} = 0.7$, $s_{\mathrm{Rx}} = 0.3$ and $\eta = 12.4$ for $t_{\mathrm{DRX}} = 10.24$s and ePSS using new longer ZC sequences (as QSI).

Table 4 gives the battery lifetime gain (β) for our different ePSS solutions with $t_{\mathrm{DRX}} = 10.24$s and $t_{\mathrm{DRX}} = 2261.44$s in the aforementioned scenarios. In the first scenario, a conventional battery lasting for 10 years can potentially last 10β = 10 $\times$ 1.38 = 13.8 years for $t_{\mathrm{DRX}} = 10.24$s and 10 $\times$ 1.23 = 12.3 years for $t_{\mathrm{DRX}} = 2621.44$s, when our ePSS using new longer ZC sequences (as QSI) solution is adopted. This is a substantial improvement considering that only 30% of the battery was being used for UE reception. The battery lifetime gain increases as the battery consumption share for UE reception increases. For instance, with our ePSS using new longer ZC sequences (as QSI) solution in the second and third scenarios, the battery lifetime increases to 18.5 years and 28.1 years respectively for $t_{\mathrm{DRX}} = 10.24$s and to 14.6 years and 17.9 years respectively for $t_{\mathrm{DRX}} = 2261.44$s, which is highly significant. The lowest energy efficiency gain is obtained when our ePSS using multiple PSS (not as QSI) solution is used. Even in this case the lifetime of a conventional battery lasting 10 years is extended to 12.9 years, 15.9 years and 20.9 years for the three scenarios for $t_{\mathrm{DRX}} = 10.24$s and to 11.5 years, 13.5 years and 15.8 years respectively for $t_{\mathrm{DRX}} = 2261.44$s, which is considerable. Similar to Section 5.2, the battery lifetime extension for ePSS as QSI solutions for longer DRX cycles serve as a loose lower bound since the SFN decoding gain is not included in the computation.

5.4 Analysis of ePSS transmission overhead

The periodicity of the ePSS transmission determines the overhead on the network. If the ePSS is scheduled on every radio frame like the PSS, it will consume a lot of network resources. From our simulation results (see Fig. 7), we note that m ePSS frames are required for the desired accuracy of timing detection, where $m = 3$ for ePSS using PSS and $m = 2$ for ePSS using new longer ZC sequences. If the periodicity of ePSS is t_{p} ms, the transmission consists m

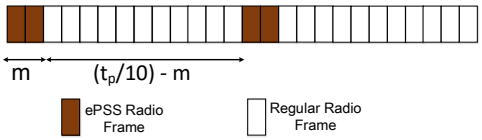

(a) Frame structure with ePSS transmission

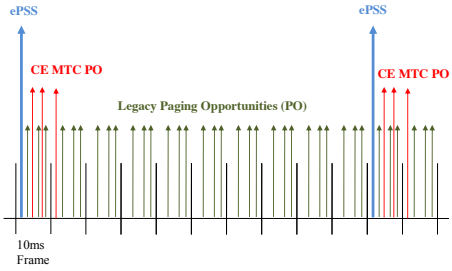

(b) ePSS and PO Allocation

Fig. 8. Frame Structure and PO Allocation for LC devices using ePSS

TABLE 5
Network resource overhead due to the ePSS transmission.

Base-station Bandwidth	t_p = 100ms	t_p= 360ms
1.4 MHz (6 PRB pairs)	[4% 6%]	[1.11% 1.67%]
5 MHz (25 PRB pairs)	[0.96% 1.44%]	[0.26% 0.4%]
10 MHz (50 PRB pairs)	[0.48% 0.72%]	[0.13% 0.2%]
20 MHz (100 PRB pairs)	[0.24% 0.36%]	[0.06% 0.1%]

ePSS radio frames followed by $(\frac{t_p}{10} - m)$ legacy radio frames as shown in Fig. 8a.

The ePSS is mostly used by the LC devices. Therefore, to minimize the resource consumption, we propose to group the paging opportunities (POs) of such UEs close to the ePSS. This solution is illustrated in Fig. 8b. For a given interval of time, the number of LC devices might a small subset of the total number of UEs. Assuming that 10% of the UEs are LC devices, the ePSS only needs to be sent every $t_p = 100$ms. Also, the paging identifier for the LC devices can be sent on the enhanced control channel (ePDCCH) [47], which uses the sub-carriers in the data channel space. The POs for the legacy UEs will be distributed and they will be paged via the regular control channel (PDCCH). This way the control channel capacity is not altered.

Moreover, when the ePSS is not transmitted every radio frame, a single ePSS will be used to resynchronize UEs that have their PO sub-frames greater than 10ms from the ePSS sub-frame. Therefore, the UE can save power by going back to sleep after successfully detecting the ePSS and wake up again just before its PO. However, we have to ensure that the UE does not lose the symbol timing (UE clock does not drift by more than 5% of the symbol time, which is 3.6μs) during its sleep time. For example, for a UE using a crystal with 10ppm accuracy, the clock drift is within 5% of a symbol if the sleep time is less than 360ms. Therefore, the maximum value of t_p is 360ms for a 10ppm accurate UE clock.

The ePSS consumes 6 PRB pairs $\times$ 2 sub-frames = 12 PRB pairs every 10ms (refer Fig. 5a). As seen from Fig. 7, the time taken to decode ePSS can be 20ms (= 24 PRB pairs for ePSS using longer ZC sequences) or 30ms (= 36 PRB pairs for ePSS using multiple PSS). The overhead on the base-station due to the resource allocation for the ePSS with periodicity $t_p = 100$ms and $t_p = 360$ms is summarized in Table 5. The numbers in each row of the second and third columns of Table 5 correspond to the network load considering ePSS decode time of 20ms and 30ms respectively. The base-station deployments usually have a bandwidth of 5MHz or more and the network overhead due to the ePSS for such base-stations is less than 1.5% for both $t_p = 100$ms and $t_p = 360$ms. Moreover, the overhead of ePSS transmission is restricted to the idle mode. The regular data transmission occurs after the UE transitions from the idle mode to the connected mode, where the resource allocation uses the default LTE/LTE-A frame structure, without the ePSS. Therefore, the ePSS does not affect the regular data transmission.

5.5 Discussion

In summary, our ePSS solutions reduced the energy consumption when compared to the legacy solutions due to the following reasons.

- The ePSS consists of an increased density of synchronization signals, i.e., ePSS packs more synchronization signals in less amount of transmission time, thereby reducing the time taken by the UE to reacquire the symbol timing.
- The ePSS has an additional attribute of being able to indicate whether there is an impending page for the UE or not, thereby helping UEs to return to sleep mode quickly when there is no page and save energy. But the legacy UE follows the procedure of decoding the paging identifier on the control channel regardless of whether it is paged or not, which is complex and energy consuming.
- The ePSS with best performance uses longer length ZC sequences, which possess better signal detection properties, thereby improving the reacquisition time and reducing power consumption.

Moreover, the legacy UE may have to reacquire the SFN so that it attempts to decode the paging information on the correct frame/sub-frame, depending on the accuracy of its clock and the length of the DRX cycle. This is because the UE will lose its frame timing when its clock drifts by more than half a frame (= $\frac{10\text{ms}}{2} = 5$ms). For example, an LC UE with 10ppm accurate clock [13] will lose its frame timing if it sleeps for more than $\frac{5\text{ms}}{(10 \cdot 10^{-6})} = 500$s. When the DRX cycle length is than 500s, the clock drift results in a symbol timing offset, but the UE remains in the same radio frame. However when the DRX cycle is longer than 500s, both the frame timing and the symbol timing are lost and the UE has to reacquire the SFN.

The SFN field in LTE/LTE-A consists of 10 bits and is incremented by one every 10ms (= frame length) [28], [31]. Hence the maximum time length that can be indicated by the SFN field is $2^{10} \times 10^{-3} = 10.24$s. In order to support extended DRX cycles, the on-going standardization activities in LTE/LTE-A have included a new field called the Hyper System Frame Number (H-SFN) which incremented by one every 10.24s [14]. Currently, the number of H-SFN bits is set to 8. Consequently, the maximum time length that can be indicated with the combination of H-SFN and the legacy SFN is $(2^8 - 1) \times 10.24 + 10.24 = 2621.44$s, which corresponds to the maximum extended DRX cycle length.

The UE has to decode the H-SFN and the SFN if it sleeps so long that the frame timing is lost, and then attempt the paging decode on the correct paging frame/sub-frame. Owing to the low operating SNR, H-SFN/SFN decoding can take multiple repetitions, increase the ON time and the energy consumption of the UE. Also, the legacy UE needs to perform this decoding even when there is no page because it can know about the validity of the page only when it decodes the paging control information (which is post H-SFN/SFN decoding). But, when our ePSS as QSI solutions are used, the UE is informed about the validity of the page during the timing resynchronization phase itself and H-SFN/SFN decoding would not be necessary when there is no page. The savings obtained from not decoding the H-SFN/SFN when there is no page has not been included in our calculations for the energy efficiency gain and battery lifetime extension. Therefore, our results for this case serve as a loose lower bound and the actual gains that can be obtained using our solutions can be higher when the DRX cycle length is longer (>500s for an LC UE with 10ppm accurate clock).

Furthermore, our ideas can be extended to other OFDM based systems where the conventional methods of CP correlation and reference signal detection take a long time to converge at very low SNR. For example, in WLAN, two new, closely spaced, robust preamble sequences can be assigned to each UE, one indicating a "Page" and the other indicating "No Page". This mapping of paging indication to resynchronization sequences, combined with shrewd resource allocation would result in an energy efficient operation of the MTC UEs.

6 Conclusion

In this paper, we considered the DRX mechanism in LTE/LTE-A for the MTC UEs requiring coverage enhancement. Firstly, we showed that the paging decode operation which is a critical part of the DRX mechanism, is very sensitive to timing offset. Secondly, we explored the conventional timing acquisition algorithms - CP autocorrelation and the legacy synchronization signal detection and demonstrated they take around 600ms and 380ms respectively for reacquiring the symbol timing within tolerable limits. This leads to increased ON time of the UE and hence results in increased energy consumption. To mitigate this problem, we introduced the Enhanced Primary Synchronization Signal (ePSS) within the LTE/LTE-A standardization framework and proposed a novel DRX mechanism which uses our ePSS for faster timing resynchronization and reduced energy consumption. We described two simple methods to design the ePSS signal - by using multiple PSS sequences and by using new ZC sequences and indicated that our ePSS design requires less than 1.5% network resource overhead for base-station bandwidths of 5MHz or more. We also proposed the use of the ePSS as the Quick Sleeping Indication (QSI) (introduced in our previous work) to further improve the energy efficiency of the LC devices. We illustrated that the modified DRX mechanism for the LC devices using our ePSS solutions are more energy efficient than the legacy mechanism. A detailed analysis of the resource allocation, higher layer signaling aspects for the ePSS and developing improved UE grouping strategies to handle higher density of LC devices constitute our future work.

References

[1] D. Astely, E. Dahlman, G. Fodor, S. Parkvall, and J. Sachs, "LTE release 12 and beyond," *IEEE Commun. Mag.*, vol. 51, no. 7, 2013.
[2] T. Taleb and A. Kunz, "Machine type communications in 3GPP networks: potential, challenges, and solutions," *IEEE Commun. Mag.*, vol. 50, no. 3, pp. 178–184, 2012.
[3] S.-Y. Lien, K.-C. Chen, and Y. Lin, "Toward ubiquitous massive accesses in 3GPP machine-to-machine communications," *IEEE Commun. Mag.*, vol. 49, no. 4, pp. 66–74, 2011.
[4] A. G. Gotsis, A. S. Lioumpas, and A. Alexiou, "M2M scheduling over LTE: Challenges and new perspectives," *IEEE Veh. Technol. Mag.*, vol. 7, no. 3, pp. 34–39, 2012.
[5] Y. Chen and W. Wang, "Machine-to-Machine communication in LTE-A," in *Proc. IEEE 72nd Veh. Technol. Conf.-Fall*, 2010, pp. 1–4.
[6] F. Ghavimi and H.-H. Chen, "M2M Communications in 3GPP LTE/LTE-A Networks: Architectures, Service Requirements, Challenges, and Applications," *IEEE Commun. Surveys Tuts.*, 2015.
[7] A. Rajandekar and B. Sikdar, "A Survey of MAC Layer Issues and Protocols for Machine-to-Machine Communications," *IEEE Internet of Things Journal*, vol. 2, no. 2, pp. 175–186, 2015.
[8] M. R. Palattella, M. Dohler, A. Grieco, G. Rizzo, J. Torsner, T. Engel, and L. Ladid, "Internet of Things in the 5G Era: Enablers, Architecture, and Business Models," *IEEE J. Sel. Areas Commun.*, vol. 34, no. 3, pp. 510–527, 2016.
[9] Researchmoz.us, "Low Power Wide Area Internet of Things (LPWA-IoT) Market Forecasts to 2020 and MNO Approaches," Apr. 2016. [Online]. Available: https://globenewswire.com/news-release/2016/04/20/830694/0/en/Low-Power-Wide-Area-Internet-of-Things-LPWA-IoT-Market-Forecasts-to-2020-and-MNO-Approaches-Researchmoz-us.html
[10] 3GPP, "Study on provision of low-cost Machine-Type Communications (MTC) User Equipments (UEs) based on LTE," 3GPP, TR 36.888, Jun. 2013.
[11] ——, "Study on Machine-Type Communications (MTC) and other mobile data applications communications enhancements," 3GPP, TR 23.887, Dec. 2013.
[12] F. Riehle, *Frequency standards: basics and applications*. John Wiley & Sons, 2006.
[13] Qualcomm Incorporated, "R4-141241 - Reply LS on AGC and Frequency Error for D2D, GPP TSG-RAN WG2 Meeting 57bis, St. Julians, Malta 26 - 30 March 2007."
[14] 3GPP, "Technical Specification Group Services and System Aspects; Architecture enhancements to facilitate communications with packet data networks and applications (Release 13)," 3GPP, TS 23.682, Mar. 2016.
[15] J.-J. Van de Beek, M. Sandell, P. O. Borjesson *et al.*, "ML estimation of time and frequency offset in OFDM systems," *IEEE Trans. Signal Process.*, vol. 45, no. 7, pp. 1800–1805, 1997.
[16] M. Speth, F. Classen, and H. Meyr, "Frame synchronization of OFDM systems in frequency selective fading channels," in *Proc. IEEE 47th Veh. Technol. Conf.*, vol. 3, 1997, pp. 1807–1811.
[17] W. Xu and K. Manolakis, "Robust synchronization for 3GPP LTE system," in *Proc. IEEE Global Telecommun. Conf.*, 2010, pp. 1–5.
[18] C.-L. Chen and S.-G. Chen, "Non-coherent cell identification detection methods and statistical analysis for OFDM systems," *IEEE Trans. Commun.*, vol. 58, no. 11, pp. 3231–3243, 2010.
[19] F. Berggren and B. M. Popović, "A non-hierarchical cell search scheme," in *Proc. IEEE Wireless Commun. and Netw. Conf.*, 2007, pp. 2300–2304.
[20] J.-W. Lee and Y.-H. Lee, "Rapid cell search in OFDM-based cellular systems," in *Proc. IEEE 61st Veh. Technol. Conf.-Spring*, vol. 2, 2005, pp. 1273–1277.
[21] C. Y. Ho and C.-Y. Huang, "Energy-saving massive access control and resource allocation schemes for M2M communications in OFDMA cellular networks," *IEEE Wireless Commun. Lett.*, vol. 1, no. 3, pp. 209–212, 2012.
[22] H. S. Dhillon, H. C. Huang, H. Viswanathan, and R. A. Valenzuela, "Power-efficient system design for cellular-based machine-to-machine communications," *IEEE Trans. Wireless Commun.*, vol. 12, no. 11, pp. 5740–5753, 2013.
[23] Y. Yuan, Z. Zuo, Y. Guan, X. Chen, W. Luo, Q. Bi, P. Chen, and X. She, "LTE-Advanced coverage enhancements," *IEEE Commun. Mag.*, vol. 52, no. 10, pp. 153–159, 2014.

[24] Y. Zhou, T. Zhang, Z. Zeng, Y. Li, and Y. Han, "LTE Uplink Coverage Enhancement Techniques Based on Enhanced TTI Bundling," in *Proc. IEEE Int. Conf. on Wireless Commun., Netw. and Mobile Comput.*, 2012, pp. 1–4.

[25] G. Naddafzadeh-Shirazi, L. Lampe, G. Vos, and S. Bennett, "Coverage enhancement techniques for machine-to-machine communications over LTE," *IEEE Commun. Mag.*, vol. 53, no. 7, pp. 192–200, 2015.

[26] Q. Mu, L. Liu, H. Jiang, and S. Yasukawa, "A new physical downlink control channel design for MTC in LTE-Advanced," in *Proc. IEEE Int. Symp. on Wireless Personal Multimedia Commun.*, 2014, pp. 294–299.

[27] C. S. Bontu and E. Illidge, "DRX mechanism for power saving in LTE," *IEEE Commun. Mag.*, vol. 47, no. 6, pp. 48–55, 2009.

[28] 3GPP, "Evolved Universal Terrestrial Radio Access (E-UTRA); Medium Access Control (MAC) protocol specification," 3GPP, TS 36.321, Mar. 2014.

[29] ——, "Evolved Universal Terrestrial Radio Access (E-UTRA); User Equipment (UE) procedures in idle mode," 3GPP, TS 36.304, Mar. 2014.

[30] ——, "Evolved Universal Terrestrial Radio Access (E-UTRA); Physical layer procedures," 3GPP, TS 36.213, Mar. 2014.

[31] H. Holma and A. Toskala, *LTE for UMTS: Evolution to LTE-Advanced*. John Wiley & Sons, 2011.

[32] T. Tirronen, A. Larmo, J. Sachs, B. Lindoff, and N. Wiberg, "Reducing energy consumption of LTE devices for machine-to-machine communication," in *Proc. IEEE Global Telecommun. Conf. Wkshps.*, 2012, pp. 1650–1656.

[33] L. Zhou, H. Xu, H. Tian, Y. Gao, L. Du, and L. Chen, "Performance analysis of power saving mechanism with adjustable DRX cycles in 3GPP LTE," in *Proc. IEEE 68th Veh. Technol. Conf.-Fall*, 2008, pp. 1–5.

[34] K. Zhou, N. Nikaein, and T. Spyropoulos, "LTE/LTE-A discontinuous reception modeling for machine type communications," *IEEE Wireless Commun. Lett.*, vol. 2, no. 1, pp. 102–105, 2013.

[35] S. Jin and D. Qiao, "Numerical analysis of the power saving in 3GPP LTE advanced wireless networks," *IEEE Trans. Veh. Technol.*, vol. 61, no. 4, pp. 1779–1785, 2012.

[36] A. T. Koc, S. C. Jha, R. Vannithamby, and M. Torlak, "Device power saving and latency optimization in LTE-A networks through DRX configuration," *IEEE Trans. Wireless Commun.*, vol. 13, no. 5, pp. 2614–2625, 2014.

[37] C. Tseng, H. Wang, F. Kuo, K. Ting, H. Chen, and G. Chen, "Delay and Power Consumption in LTE/LTE-A DRX Mechanism with Mixed Short and Long Cycles," *IEEE Trans. Veh. Technol.*, vol. PP, no. 99, pp. 1–1, 2015.

[38] S. C. Jha, A. T. Koc, and R. Vannithamby, "Device power saving mechanisms for low cost MTC over LTE networks," in *IEEE Int. Conf. on Commun. Wkshps.*, 2014, pp. 412–417.

[39] P. Osti, P. Lassila, S. Aalto, A. Larmo, and T. Tirronen, "Analysis of PDCCH performance for M2M traffic in LTE," *IEEE Trans. Veh. Technol.*, vol. 63, no. 9, pp. 4357–4371, 2014.

[40] P. Frenger, H. Koorapaty, and J.-C. Guey, "Evaluation of control channel performance with adaptive radio unit activation in LTE," in *Proc. IEEE 75th Veh. Technol. Conf.-Spring*, 2012, pp. 1–5.

[41] J. Milos and S. Hanus, "Performance analysis of PCFICH and PDCCH LTE control channels," *Radioengineering*, vol. 23, no. 1, 2014.

[42] J. Zhu and H. Li, "On the performance of LTE physical downlink shared channel," in *Proc. IEEE Int. Conf. on Comput. Sci. and Netw. Technol.*, vol. 2, 2011, pp. 983–986.

[43] N. M. Balasubramanya, L. Lampe, G. Vos, and S. Bennett, "Introducing quick sleeping using the broadcast channel for 3GPP LTE MTC," in *Proc. IEEE Global Telecommun. Conf. Wkshps.*, 2014, pp. 606–611.

[44] 3GPP, "Evolved Universal Terrestrial Radio Access (E-UTRA); Physical channels and modulation," 3GPP, TS 36.211, Mar. 2014.

[45] ——, "Evolved Universal Terrestrial Radio Access (E-UTRA); Multiplexing and channel coding," 3GPP, TS 36.212, Dec. 2013.

[46] ——, "User Equipment (UE) Radio Transmission and Reception." 3GPP, TS 36.101, Mar. 2014.

[47] S. Ye, S. H. Wong, and C. Worrall, "Enhanced physical downlink control channel in LTE Advanced Release 11," *IEEE Commun. Mag.*, vol. 51, no. 2, pp. 82–89, 2013.

[48] Nokia, "R2-071285 - DRX parameters in LTE, 3GPP TSG-RAN WG4 Meeting 70, San Francisco, USA, 10th-14th Feb., 2014."

[49] S. Fowler, "Study on power saving based on radio frame in LTE wireless communication system using DRX," in *Proc. IEEE Global Telecommun. Conf. Wkshps.*, 2011, pp. 1062–1066.

[50] R. Yavne, "An economical method for calculating the discrete Fourier transform," in *Proc. of Fall Joint Comput. Conf., Part I*, Dec, pp. 115–125.

[51] Y. Lin, H. Lee, M. Woh, Y. Harel, S. Mahlke, T. Mudge, C. Chakrabarti, and K. Flautner, "Soda: A low-power architecture for software radio," *ACM SIGARCH Comput. Arch. News*, vol. 34, no. 2, pp. 89–101, 2006.